The Co–Au interface in bimetallic nanoparticles: a high resolution STEM study

Alvaro Mayoral,[a] Sergio Mejía-Rosales,[ab] Marcelo M. Mariscal,[c] Eduardo Pérez-Tijerina[b] and Miguel José-Yacamán*[a]

Received 14th July 2010, Accepted 1st September 2010
DOI: 10.1039/c0nr00498g

We report the formation of Au/Co nanoparticles and their characterization by aberration (C_s) corrected scanning transmission electron microscopy (STEM). The nanoparticles were synthesized by inert gas condensation, forming initially core-shell and bimetallic crystals. However, after thermal treatment at normal atmospheric conditions, the Co nanoparticles changed their morphology into a fine layer forming a perfect interface with the gold. The ordering of the zone rich in Co presents a *fcc* arrangement matching the gold lattice. The atomic analysis on the interface and the comparison of the STEM images with numerical simulations corroborated the atomic substitution of gold by cobalt.

Introduction

Metal nanoparticles composed by two or more metals have unique optical, electrical and catalytic properties.[1–4] Moreover, in the field of heterogeneous catalysis, bimetallic nanoparticles constitute a promising type of catalyst as properties of the material can be related with the elements forming the nanoparticles.[5] The integration of two or more metals into the same particle is therefore highly desirable as these materials can accomplish more than one function at the time. A good example of this effect would be that of magnetic metals such as Co, alloyed with non-magnetic materials that introduce catalytic or optical effects into the final product. Thus, it has been found that catalytic and magnetic properties can be combined and tuned in Co/Pt systems,[6] and optical properties can be exploited in Au/Co nanoparticles.[7] Moreover, the observation of giant magnetoresistance in systems built from magnetic and non-magnetic solids has renewed the interest devoted to these materials. [8]

Unfortunately, the analysis at atomistic level of small bimetallic nanoparticles has remained a challenge during the past years, since high resolution electron microscopy was limited by aberrations produced by the lenses inside the column. With the development of aberration corrected transmission electron microscopes, atomic resolution can be achieved on scanning transmission mode (STEM) and, therefore, smaller dimensions that could not be resolved by conventional electron microscopy techniques can now be directly imaged.[9,10] By combining this mode with a high angle annular dark field (HAADF) detector, where the contrast on the image roughly depends on Z^n (where n has a value close to 2), it is possible to locate elements on the materials based only on their difference in atomic weight.[11,12] This direct interpretation is of particular interest in the catalysis field, as bimetallic nanoparticles are used in several reactions such as CO oxidation, hydrogenation of hydrocarbons, and synthesis of vinyl acetate, among others.[4,13–15] Nowadays, probes smaller than 1 Å can be achieved, single atoms can be imaged, and the structure and shape of small nanoparticles of just a few nanometers can be identified.

Among the different methods for producing bimetallic nanoparticles, those based on chemical procedures are the most commonly used,[16,17] with the particles produced by these methods commonly having core shell structure[18,19] and icosahedral or cuboctahedral geometries; however, the particles may also form truncated octahedra or decahedra. Physical methods usually allow better control of the size and shape of the particles, which make them the best choice when these properties are critical for a specific application. In the present work the production of Au and Co nanoparticles has been achieved using a sputtering system, where the particles are nucleated in the presence of a coolant inert gas.[20] The resulting nanoparticles were analyzed by means of aberration corrected scanning transmission electron microscopy, using HAADF and bright field (BF) detectors, and the chemical composition was confirmed by EDX analysis. In addition, one of the microgrids supporting the particles was heated at normal atmospheric conditions, in order to study the effect of the heating process in the distribution and chemical composition of both metals.

Experimental

Bimetallic Au/Co nanoparticles were produced with a sputtering system Nanogen 50 from Mantis Deposition Ltd.[21] using what is known as the Inert Gas Condensation method (IGC).[22,23] In the IGC process, a supersaturated vapor of metal atoms is generated by sputtering a metal target in an inert gas atmosphere of Ar and He. The Nanogen 50 system was kept at low temperature by a coolant mixture, and before the deposition of the nanoparticles the system pressure was set at 1×10^{-9} Torr. The production rate and size of the nanoparticles were controlled through the variation of the gas flow, the partial pressure, the magnetron power, and the condensation zone length. These parameters were

[a]*Department of Physics and Astronomy, The University of Texas at San Antonio, One UTSA Circle, 78251 San Antonio, Texas, USA. E-mail: Miguel.yacaman@utsa.edu*
[b]*Laboratorio de Nanociencias y Nanotecnología, Facultad de Ciencias Físico-Matemáticas, Universidad Autónoma de Nuevo León, San Nicolás de los Garza, Nuevo León, 66450, México*
[c]*INFIQC/CONICET, Departamento de Matemática y Física, Facultad de Ciencias Químicas, Universidad Nacional de Córdoba, Córdoba, Argentina*

optimized to produce particles of 5.0 nm in size. The nanoparticles were deposited directly onto holey carbon copper microgrids.

One of the microgrids was heated in a furnace up to 275 °C for 12 h using a ramp rate of 2 °C/min. After the thermal treatment, the sample was cooled to room temperature by taking the grid out of the furnace.

The materials obtained were characterized in a JEOL JEM-ARM200F electron microscope. STEM images were simultaneously recorded in both HAADF and BF modes with the microscope operating at 200 kV. The probe correction was performed through a dodecapole corrector (CEOS GmbH) aligned through the CESCOR software, to finally obtain a twelve-fold ronchigram with a flat area of 50 mrad. The HAADF images were obtained setting the annular detector lower and higher scattering semi-angles to 68 to 280 mrad respectively, easily satisfying the requirement for the detector to eliminate contributions from unscattered or low-angle scattered electrons. The pixel spacing was calibrated using Si 110 lattice images in HAADF mode, and confirmed by using gold standard particles. Images were commonly recorded for 10 to 16 s.

Results and discussion

The particle size, before any thermal treatment, was found to be around 5 nm, but with frequent agglomeration into larger crystals due to the high deposition times. Fig. 1a displays an aberration (C_s) corrected HAADF image of the as-synthesized product composed of gold (bright regions) and cobalt nanoparticles (dark regions) presenting in most of the cases five fold symmetry (icosahedra or decahedra). Fig. 1b presents two non-agglomerated nanoparticles; the particle at the top of the image is a Co icosahedron of approximately 3 nm observed along the [110] orientation, with a d-spacing in the last layer of {111} planes of 0.231 nm. At the bottom of the image, the brighter Au particle is a decahedron of 4.5 nm, orientated along the [110] direction, with $d_{\{111\}} = 0.255$ nm. A preliminary inspection showed that these two geometries were dominant in the whole of the sample.

Due to the small size and the facility of cobalt to be oxidized it is expected that for the case of cobalt crystals or cobalt rich zones the material was partially or totally oxidized into cobalt oxide.

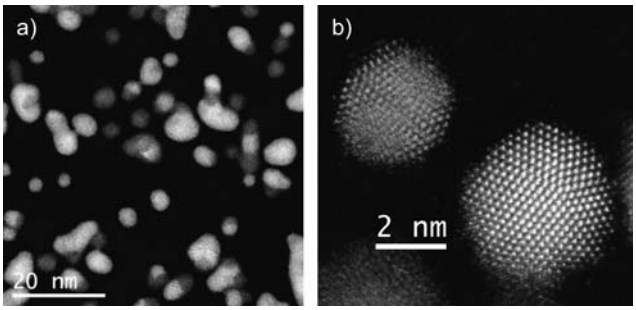

Fig. 1 Cs corrected STEM-HAADF images of a) several bimetallic nanoparticles and b) Co icosahedral nanoparticle along the two-fold axis on top and Au decahedral nanoparticle presenting a five-fold symmetry, bottom and bright.

When the agglomeration of two particles happened it usually occurred in one of two possible ways: the first and the most commonly observed was when two particles coalescence through one of the faces (as shown in Fig. 2a) forming a bimetallic nanoparticle with one side rich in Au and the other rich in Co; the second way is through the rearrangement of the particles into a core-shell structure (as in Fig. 2c), where the core of the particle is made of gold and the cobalt oxide partially or totally covers the surface. The intensity profile shown in Fig. 2b, corresponding to the region marked in Fig. 2a, shows how different are the intensities due to the two metals.

After the preliminary observation of the structures, the same microgrid was heated for 12 h at 275 °C and finally was quenched to room temperature by taking it out from the furnace. The grid, which was in a good condition after the process, was re-observed under the microscope. The STEM images of the sample at low magnification revealed that the gold nanoparticles seemed to remain without significant changes after the process. In contrast, the Co nanoparticles had completely changed their morphology, with a thin layer of material spread over the grid. This layer, which originally was thought to be either amorphous Co or impurities from the heating process, was indeed an ordered crystal structure, as can be noted in Fig. 3b.

The high-resolution analysis performed on this sample revealed some unexpected features about the way the metals were linked to each other. Fig. 4 displays a gold decahedral nanoparticle after the thermal treatment, showing the raw STEM intensity signal. The FFT diffractogram, shown inset in the figure, proves the high degree of crystallinity of the material and its five-fold symmetry, as the particle is lying on its zone axis perpendicular to the electron beam. Because of its orientation, it is possible to confirm that the particle is formed by 5 domains with different size, intersected by twin planes, which in each case present a structure free of defects. Three of the corners resemble the shape of a Marks decahedron, while an extra {100} facet can be also identified on another corner.

Gold atomic vacancies can be also identified in different parts of the crystal. Fig. 5a shows an enlarged area of the particle shown in Fig. 4, where Co atoms fill the Au vacancies (right side of the tetrahedron identified with a triangle in the figure). At the bottom part of the particle four atomic columns made of gold atoms have vacancies between them (Fig. 5b), and all these vacancies are filled with less bright columns, which are attributed to Co. The vacancies as well as the last layer of Au atoms are perfectly alloyed with the Co regions. The areas rich in cobalt retained the same symmetry as gold (along the [110] orientation) and also the same distance in the adjacent layer, just at the interface (Fig. 5c). However, the interatomic distances measured for cobalt are not in agreement with the Co at bulk, but they are closer to those expected in cobalt oxide CoO.[24] This good agreement is apparent in Fig. 5b, where we have superimposed a ball-and-stick model of a fragment of the lattice of CoO. The composition was confirmed by EDX analysis: Fig. 6 shows the compositional maps of Au (Fig. 6b), Co (Fig. 6c), O (Fig. 6d), performed on 4 nm Au nanoparticles (Fig. 6a). The oxygen signal appears to be spread along the sample, but, due to the oxygen is a relatively light element and therefore more difficult to be detected by EDX analysis, it is not uncommon that the O maps are more diffused than those obtained for heavy atoms. From the

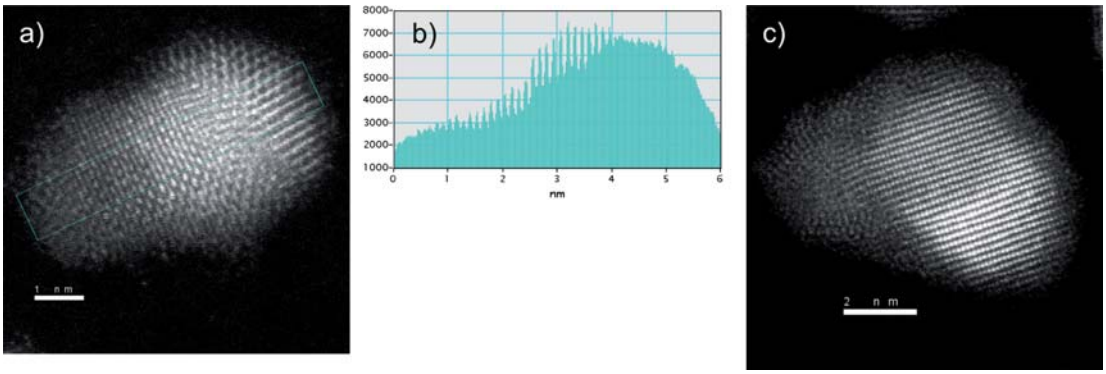

Fig. 2 C_s corrected STEM-HAADF images of a) Au/Co nanoparticle with a cobalt rich zone (left) and gold rich zone (right). b) Intensity profile (in arbitrary units) of the area marked in a) showing the dramatic difference in the intensity due to the difference in the atomic number. c) Au/Co nanoparticle recorded along the [211] orientation, where gold (bright zone) is in the core surrounded by Co.

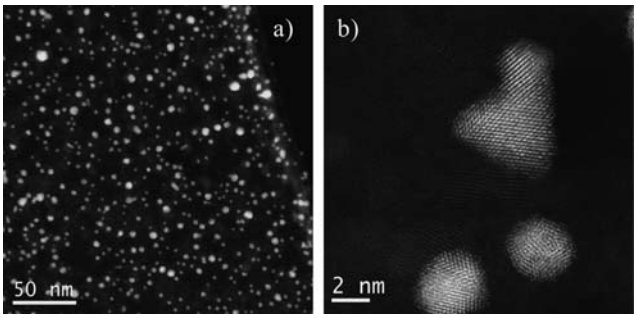

Fig. 3 C_s corrected STEM-HAADF images of Au/Co after heating, a) low magnification image and b) high resolution data showing the crystallinity of both materials.

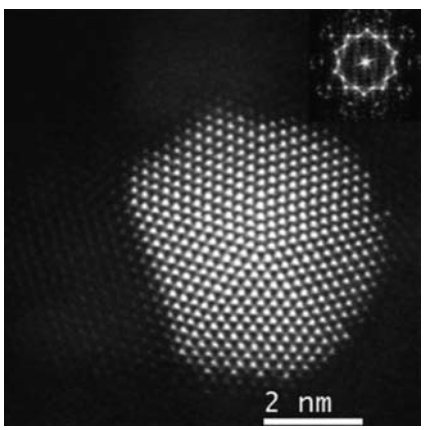

Fig. 4 C_s corrected STEM-HAADF image of a decahedral Au nanoparticle (raw data).

figure it can be noted that the O map intensity signal is higher in the areas where the cobalt is present, and that these areas are located on the surroundings of the Au-rich regions, which confirms that the CoO is indeed surrounding the Au nanoparticles.

In HAADF-STEM micrographs, the intensity signal depends on the atomic number Z of the element present in the atomic column parallel to the electron beam. It is then expected that the cobalt columns generate a less intense signal than those made of Au, both because of the difference in Z, and because the difference in the height of the atomic columns. We performed a HAADF-STEM simulation of atomic columns of Au and Co to calculate these differences in intensity. The HAADF-STEM simulations were performed using the multislice method, as implemented on the STEM Image Simulation module of the xHREM suite by HREM Research Inc.[25] The simulation results for columns with less than 7 atoms in thickness are shown in Fig. 7. Here, we can note that when a Co atomic column is 5 to 7 atoms thick, it will be represented in the micrograph with an intensity that is only 15 to 20% of the value of an Au column containing the same numbers of atoms. For columns larger than 7 atoms, the relation between intensity and thickness is not always monotonic, but for the sizes, shapes, and chemical distributions of the particles studied here, the assumption that at the Au–Co interface the columns are around 7 atoms thick is justified.

Based on the comparison presented in Fig. 7, we prepared a rough model of the particle of Fig. 4 and 5, in order to investigate the Au–CoO interface. The model, shown in Fig. 8b, consists of a decahedral gold particle, surrounded by several layers of CoO that match the structure of gold, following the main trends of the intensity profile shown in false colors in Fig. 8a. The model does not intend to represent the real shape of the particle—the shape of the particle of Fig. 4 is obviously not a perfect decahedron—but to propose an adequate description of the interface between the two metals. We centered our attention on the region marked with a white square in Fig. 8 (roughly the same shown in Fig. 5c), where the CoO atomic layers are well defined. The HAADF-STEM simulation of this region, along with its comparison with the real micrograph, is shown in Fig. 9. From the comparison between the intensity profiles Fig. 9a and 9b, marked in the real and simulated micrographs by straight lines, we can infer that the Co layers indeed arrange themselves following the *fcc* structure of Au.[26,27]

The oxidation of Co and the lack of reaction of Au with oxygen can be explained in terms of the free energy change (ΔG^f) accompanying the formation of an oxide. While most metals show a negative free energy of oxide formation and react with oxygen, Au has a positive $\Delta G^f = +10.5$ kcal/O atom at 227 °C), and therefore metallic Au^0 is stable when exposed to air.[28]

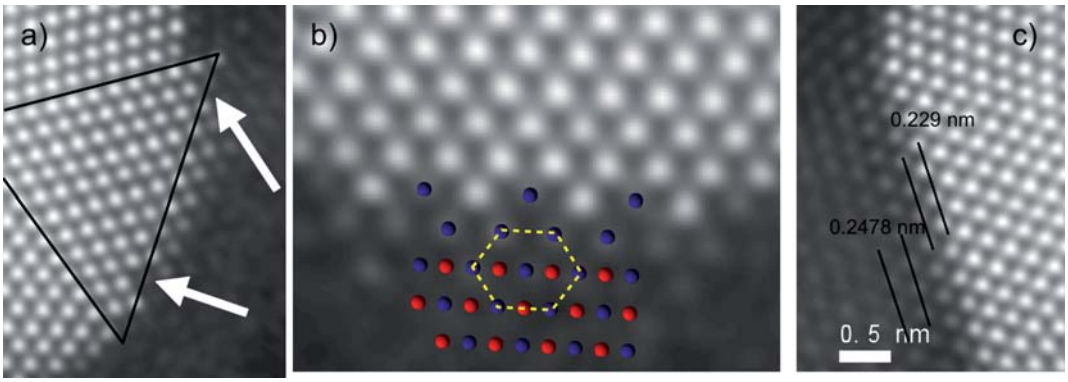

Fig. 5 Atomic resolution C_s corrected STEM-HAADF images of a) Au vacancies, where the alloying happens. b) Au–Co interface, with a ball-and-stick model of CoO superimposed on the region rich in cobalt (blue: Co atoms; red: O atoms). c) Interface between Au and Co and the characteristic distances between different atomic layers.

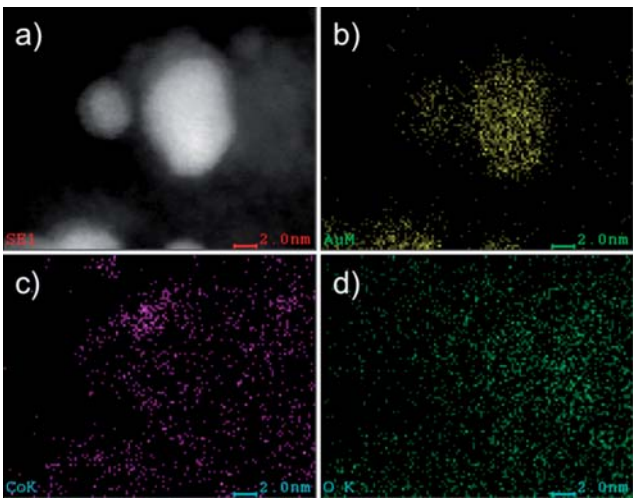

Fig. 6 EDX analysis of the nanoparticles after the thermal treatment. a) STEM-HAADF image used as reference. b) Elemental map of Au. c) Elemental map of Co. d) Elemental map of O.

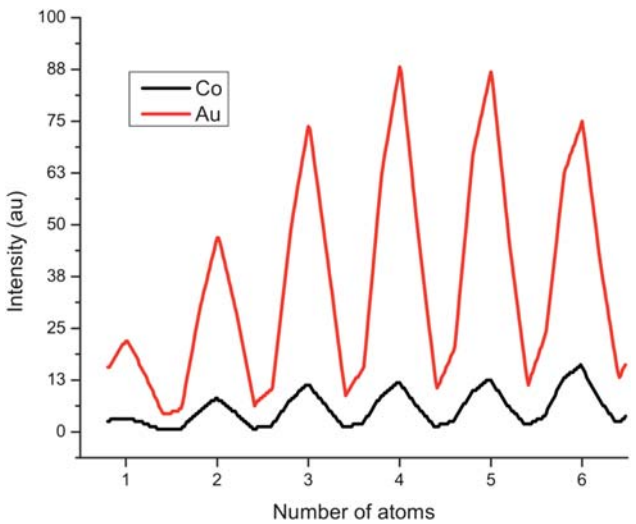

Fig. 7 Simulated HAADF-STEM signal for atomic columns of different heights.

The case of cobalt is different due that the ΔG^f for CoO formation is −95 kcal/O at 275 °C,[29] confirming, from thermodynamics basis, that the oxide formation is highly stable.

Concerning the substrate effect during the annealing process, we believe that the substrate surface does not influence considerably the stability of the nanoparticles. This is supported by theoretical calculations reported for several metallic nanoparticles onto carbon-based surfaces. For instance, the adsorption energy of Au with graphite surfaces is 0.096 eV,[30] considerably smaller than the 3.9 eV of the Au–Au interaction.

Clearly, the thermal treatment in the presence of oxygen had a strong influence on the Co nanoparticles morphology, as significant changes have been found before and after the reaction. According to our results, Au nanoparticles seem to be more temperature stable compared with the same size cobalt oxide crystals. After heating, as a result of the presence of oxygen and temperature the cobalt oxidized forming an interface which was more easily identified. For the case of gold, some atoms are either released or relocated from their original sites at the surface of the particles, leaving some vacancies filled by Co atoms.

Another aspect worth mentioning is the asymmetry observed in the decahedron presented in Fig. 4. It is well known that these kinds of five-fold symmetry particles are not equilibrium crystals and different methods for releasing that tension and making them stable have been discussed.[31] In this experiment after the heating process this decahedron is expected to be more stable than the original material and such stabilization might be provided by a larger size of one of the tetrahedra conforming the material and the formation of an extra face.

Conclusions

In summary, 5 nm Au/CoO nanoparticles have been synthesized by a gas condensation technique. The material, which was analyzed using aberration corrected STEM, seemed to originally form core-shell and bimetallic nanoparticles. After heating, it was found that the structures of Au were more stable than those of CoO, which diffused along the microgrid forming a very fine layer. In the vicinity of the gold regions, the cobalt oxide lattice is a pseudomorph of the Au *fcc* lattice. This effect allows us to

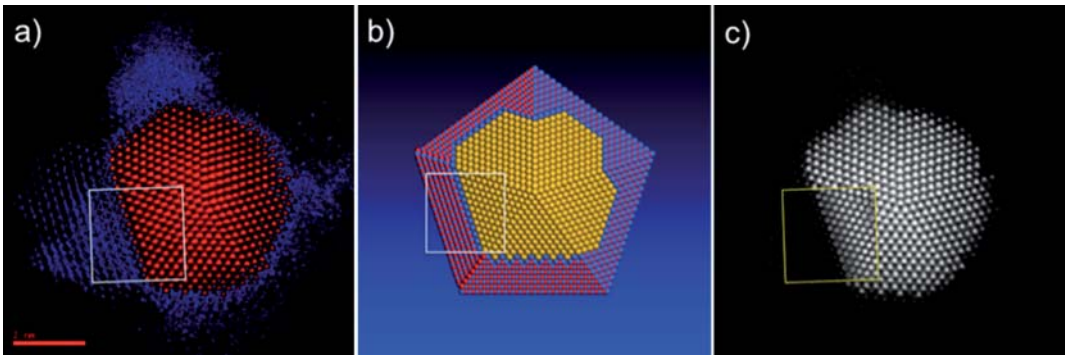

Fig. 8 a) Particle shown in the STEM micrograph of Fig. 4, redrawn in false colors according to intensity. Red color corresponds to gold atoms; blue to cobalt. b) Atomistic model that describes the Au–CoO interface of the particle shown in Fig. 4 and 5. Yellow spheres represent gold atoms; blue spheres are cobalt, and red spheres are oxygen atoms. (c) Particle shown in the STEM micrograph of Fig. 4. The region marked by the yellow square is the simulated STEM intensity map corresponding to the white square on the model shown in (b).

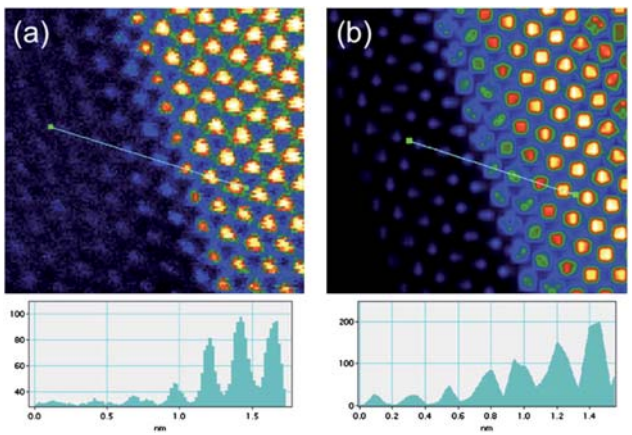

Fig. 9 Artificially coloured C_s corrected STEM micrographs: a) raw data and b) simulated image. The intensity profiles (arbitrary units) corresponding to the line drawn on the figures are also presented.

observe at atomic detail and for the very first time the interface of both metals.

Acknowledgements

The authors would like to thank NSF grant award DMR-0830074: "Alloys at the Nanoscale: The Case of Nanoparticles", and the Welch Foundation grant award AX-1615: "Controlling the Shape and Particles Using Wet Chemistry Methods and its Application to Synthesis of Hollow Bimetallic Nanostructures". We also recognize CONACYT and CONICET and PREM-NSF at UTSA for funding, C. Gutiérrez-Wing (ININ, Mexico) for her insightful comments, and D. Olmos for his technical support.

Notes and references

1 P. Mulvaney, M. Giersig and A. Henglein, *J. Phys. Chem.*, 1993, **97**(24), 6334–6336.
2 H. Yasuda, T. Kameoka, T. Sato, N. Kijima and Y. Yoshimura, *Appl. Catal. A*, 1999, **185**, L1999–L1201.
3 G. Schmid, H. West, J. O. Malm and C. Grenthe, *Chem.–Eur. J.*, 1996, **2**, 1099–1103.
4 V. Caps, S. Arrii, F. Morfin, G. Bergeret and J. L. Rousset, *Faraday Discuss.*, 2008, **138**, 241–256.
5 R. Wang, O. Dmitrieva, M. Farle, G. Dumpich, M. Acet, S. Mejia-Rosales, E. Perez-Tijerina, M. J. Yacaman and C. Kisielowski, *J. Phys. Chem. C*, 2010.
6 B. H. An, J. H. Wu, H. L. Liu, S. P. Ko, J.-S. Ju and Y. K. Kim, *Colloids Surf.*, 2008, **250**, 313–314.
7 H. L. Liu, C. H. Sonn, J. H. Wu, K.-M. Lee and Y. K. Kim, *Biomaterials*, 2008, **29**, 4003.
8 P. M. Levy, *Solid State Phys.*, 1994, **47**, 367.
9 Z. Y. Li, N. P. Young, M. D. Vece, S. Palomba, R. E. Palmer, A. L. Bleloch, B. C. Curley, R. L. Johnston, J. Jiang and J. Yuan, *Nature*, 2008, **451**, 46.
10 P. E. Baston, N. Dellby and O. L. Krivanek, *Nature*, 2002, **418**, 617.
11 D. A. Blom, L. A. Allard, S. Mishina and M. A. O'Keefe, *Microsc. Microanal.*, 2006, **12**, 483.
12 D. Ferrer, D. A. Blom, L. F. Allard, S. Mejia, E. Perez-Tijerina and M. Jose-Yacaman, *J. Mater. Chem.*, 2008, **18**, 2442.
13 A. Jablonski, S. H. Overbury and G. A. Somorjai, *Surf. Sci.*, 1977, **65**(2), 578–592.
14 B. J. Wood and H. Wise, *Surf. Sci.*, 1975, **52**(1), 151–160.
15 C. W. Yi, K. Luo, T. Wei and D. W. Goodman, *J. Phys. Chem. B*, 2005, **109**(39), 18535–18540.
16 T. Itakura, K. Torigoe and K. Esumi, *Langmuir*, 1995, **11**(10), 4129–4134.
17 M. J. Hostetler, C. J. Zhong, B. K. H. Yen, J. Anderegg, S. M. Gross, N. D. Evans, M. Porter and R. W. Murria, *J. Am. Chem. Soc.*, 1998, **120**(36), 9396–9397.
18 I. Srnova-Sloufova, F. Lednicky, A. Gemperle and J. Gemperlove, *Langmuir*, 2000, **16**(25), 9928–9935.
19 S. J. Mejia-Rosales, C. Fernandez-Navarro, E. Perez-Tijerina, J. M. Montejano-Carrizales and M. Jose-Yacaman, *J. Phys. Chem. B*, 2006, **110**(26), 12884–12889.
20 E. Perez-Tijerina, M. G. Pinilla, S. Mejia-Rosales, U. Ortiz-Mendez, A. Torres and M. Jose-Yacaman, *Faraday Discuss.*, 2008, **138**, 353–362.
21 Mantis Deposition LTD, Oxon, OX9 3BX, U.K. http://www.mantisdeposition.com.
22 K. Sattler, J. Mühlbach and E. Recknagel, *Phys. Rev. Lett.*, 1980, **45**, 821–824.
23 I. M. Goldby, B. V. Issendorff, L. Kuipers and R. E. Palmer, *Rev. Sci. Instrum.*, 1997, **68**, 3327–3334.
24 M. Ghosh, E. V. Sampathkumaran and C. N. R. Rao, *Chem. Mater.*, 2005, **17**, 2348–2352.
25 K. Ishizuka, *Ultramicroscopy*, 2001, **90**, 71–83.
26 W. A. Jesser and J. W. Matthews, *Acta Metall.*, 1968, **16**, 1307–1311.
27 W. A. Jesser and J. W. Matthews, *Philos. Mag.*, 1968, **17**, 461–473.
28 T. F. Buehrer and W. E. Roseveare, *J. Am. Chem. Soc.*, 1989, **49**, 1927.
29 L. S. Darken and R. W. Gurry, *Physical Chemistry of Metals*, McGraw-Hill, New York, 1953.
30 K. T. Chan, J. B. Neaton and M. L. Cohen, *Phys. Rev. B: Condens. Matter Mater. Phys.*, 2008, **77**, 235430.
31 A. Mayoral, H. Barron, R. Estrada-Salas, A. Vazquez-Duran and M. José-Yacamán, *Nanoscale*, 2010, **2**, 335–342.